Available online at www.sciencedirect.com
SCIENCE DIRECT®
Surface Science 563 (2004) 74–82
SURFACE SCIENCE
www.elsevier.com/locate/susc

Cerium oxidation state in ceria nanoparticles studied with X-ray photoelectron spectroscopy and absorption near edge spectroscopy

Feng Zhang [a], Peng Wang [b], J. Koberstein [b], S. Khalid [c], Siu-Wai Chan [a,*]

[a] *Department of Applied Physics and Applied Mathematics, MRSEC, Columbia University, MC 4701, 500 W. 120th Street, New York, NY 10027, USA*
[b] *Department of Chemical Engineering, MRSEC, Columbia University, New York, NY 10027, USA*
[c] *National Synchrotron Light Source, Brookhaven National Laboratory, Upton, New York, NY 11973, USA*

Received 3 December 2003; accepted for publication 20 May 2004
Available online 26 June 2004

Abstract

X-ray photoelectron spectroscopy and X-ray absorption near edge spectroscopy experiments are used to investigate the oxidation state of cerium ions in ceria nanoparticles. A comparison of results shows that XPS yields a higher concentration of Ce^{3+} ions, even after analysis with a core–shell model. Three factors are proposed for the discrepancy between results: surface reduction of ceria in the XPS vacuum chamber enhanced by X-ray radiation, fast reduction dynamics associated with ceria nanoparticles, and a diffuse depth profile of the Ce^{3+} concentration inside ceria particles. Our results suggest that the high-vacuum XPS studies of ceria have overestimated the Ce^{3+} concentration in ceria nanoparticles under ambient condition. More importantly, we have demonstrated the importance of using complimentary surface analysis techniques to investigate the valence state of ceria nanoparticles.

Keywords: Cerium; X-ray photoelectron spectroscopy; X-ray absorption spectroscopy; Oxidation

1. Introduction

Cerium oxide (i.e. CeO_{2-y} or ceria) is used in three-way catalysts for its oxygen storage capacity [1] and in diesel fuels for a more complete combustion to abate soot formation [2]. Both usages depend on its ease of releasing oxygen in a low oxygen environment, with simultaneous reduction of some Ce^{4+} to Ce^{3+}. There are many studies of cerium oxide that employ X-ray photoelectron spectroscopy and many conclusions on the oxidation states have been drawn based on these studies [3–9]. X-ray photoelectron spectroscopy (XPS) is a powerful and sensitive surface probe that requires the samples to be in a high vacuum environment (i.e. $\sim 10^{-9}$ Torr). Some previous studies have demonstrated that prolonged X-ray exposure in XPS chamber may have caused a reduction of CeO_2 [5,6]. Several interpretations,

* Corresponding author. Tel.: +212-854-8519; fax: +212-854-8257.
E-mail address: sc174@columbia.edu (S.-W. Chan).

0039-6028/$ - see front matter © 2004 Elsevier B.V. All rights reserved.
doi:10.1016/j.susc.2004.05.138

i.e. intensive local heating by X-ray [10], X-ray damage [5], and low energy photoelectron damage [11], have been provided to explain the reduction of ceria in XPS. XPS measurements do not directly provide the concentrations of the measured elements. On the contrary, XPS results provide the Laplace transform of the actual concentration depth profile. Hence, if the oxidation state of cerium on ceria surfaces responds dynamically upon exposure to high vacuum and X-ray, some of these studies may have inferred surface properties that are not representative of ceria in ambient or in a catalytic reaction environment. X-ray absorption near edge spectroscopy (XANES) is a technique that can circumvent this XPS limitation since it can be employed in vacuum, under ambient pressure, or under high pressure. This report compares XPS and XANES results on monodispersed nanoparticles and micrometer-sized ceria powder. The dynamic effect of the oxidation state of cerium at the ceria surface is also addressed.

2. Experimental

Cerium oxide nanoparticles were prepared by mixing cerium nitrate and hexamethylenetetramine in aqueous solution at room temperature. The details of the preparation were reported earlier [12]. The prepared nanoparticles have been characterized by X-ray diffraction, high-resolution transmission electron microscopy, UV-visible light absorption, and Raman scattering [12–15]. The micron-sized ceria (99.99%) used in this study was obtained from Alfa Aesar.

The XPS samples were prepared by dispersing the ceria particles in a 10% polyvinyl alcohol (Alfa Aesar, with average molecular weight of 57 000–66 000) aqueous solution and spin-coating the solution onto silicon wafers at 4000 rpm for 1 min. The samples were dried on a hot plate at ~60 °C in air, then held in a vacuum desiccator (~60 kPa) overnight.

X-ray photoelectron spectroscopy was measured using an X-ray photoelectron spectrometer (model 5500, Perkin-Elmer Co., Ltd., USA) with a monochromatic X-ray source of Al Kα. The operating condition for recording Ce_{3d} high-resolution spectra was: 15 kV and 350 W for the Al monochromatic X-ray source; pass energy of 23.5 eV with an operating pressure of 5×10^{-9} Torr. The acquisition time is 60 min for all samples. A flood electron gun was applied to compensate for the charging due to the loss of photoelectrons with an emission current of 20 mA and electron energy of 1.0 eV. The samples were measured immediately after loading into the UAH chamber, with the exception of the micron-sized CeO_2 sample, which was kept inside the XPS high vacuum chamber overnight (without X-ray or electron irradiation) before taking measurements. The XPS operational conditions described in this paper are similar to those in [5,6], as shown in Table 1.

X-ray absorption near edge spectra (XANES) were collected at the Ce L_{III} edge using the X18B beamline at National Synchrotron Light Source, Brookhaven National Lab. The XANES samples were prepared by spreading a thin layer of particles on pieces of Scotch tape. The Si(1 1 1) double-crystal monochromater was detuned (monitored by a 30% decrease of the maximum incident intensity) to remove high order harmonic light. Micron-sized cerium (IV) oxide and cerium (III) sulfide (Alfa Aesar) were used as Ce^{4+} and Ce^{3+} standards respectively. Although both fluorescence and transmission spectra were recorded, only results from transmission mode were used in this study. All the spectra were normalized in the same way using the WINXAS software [16].

Table 1
XPS operational condition

Source	XPS source	Pressure of UHV chamber	Neutralizer
This article	Monochromatic Al Kα	$\sim5\times10^{-9}$ Torr	On
Ref. [5]	Unmonochromatic Al Kα	$\sim5\times10^{-10}$ Torr	Information not available
Ref. [6]	Monochromatic Al Kα	$\sim10^{-9}$ Torr	Information not available

3. Results

3.1. X-ray photoelectron spectroscopy

Inherent challenges have been present in use of XPS to study ceria and ceria-based materials. Several researchers have experienced problems such as charging and have presented different interpretations of the results [6–9,17]. In general, it is well accepted that 10 peaks appear for CeO_{2-x} in the Ce_{3d} XPS spectrum (shown in Table 2) [18,19]. The concentration of Ce^{3+} in ceria can be determined from the following equations [19]:

$$\mathrm{Ce(III)} = v_0 + v' + u_0 + u' \quad (1)$$

$$\mathrm{Ce(IV)} = v + v'' + v''' + u + u'' + u''' \quad (2)$$

$$[\mathrm{Ce(III)}] = \frac{\mathrm{Ce(III)}}{\mathrm{Ce(III)} + \mathrm{Ce(IV)}} \quad (3)$$

where the notations Ce(III) and Ce(IV) represent the corresponding sums of the integrated peak areas related to the Ce^{3+} and Ce^{4+} XPS signals respectively. Typical XPS spectra for CeO_2 and Ce_2O_3 are shown in Fig. 1 [13]. These authors mentioned that both spectra are similar to fully oxidized or reduced samples, indicating that they recognize that ultra high vacuum (UHV) might affect the oxygen concentration in CeO_{2-x}.

The spectrum presented in Fig. 1 consists of a number of overlapping peaks. If Gaussian functions are used to model the peaks, there are three parameters for each peak, i.e. peak position, peak intensity, and full width at half maximum. Hence, a total of 30 parameters are required to fit the entire spectrum. Although it is fairly easy to obtain a good simulation of the experimental spectrum, it is difficult to get a unique and consistent result. To circumvent the problem, we first obtained the position of the well-resolved u‴ peak in the spectrum. We then fixed other peak positions based on Table 2 to simplify the simulation. With this approach, relatively stable and consistent results were obtained.

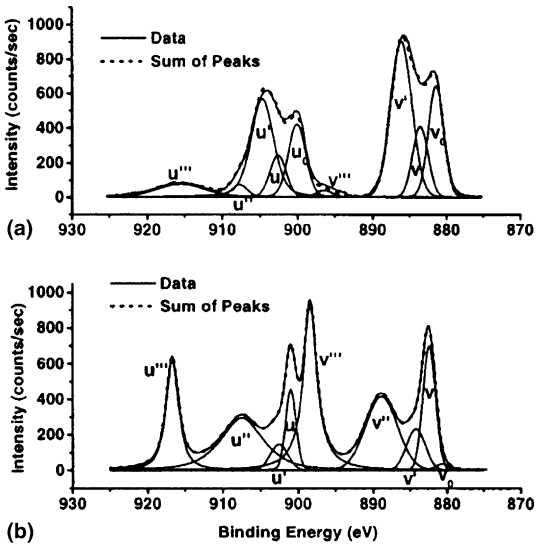

Fig. 1. (a) An XPS spectrum of well-oxidized ceria *close* to Ce_2O_3, taken from [13]. (b) An XPS spectrum of reduced ceria *close* to CeO_2, taken from [13].

Two XPS spectra of micron-sized CeO_{2-x} are shown in Fig. 2. One was taken immediately after loading the sample into the UHV chamber, while the other was taken after the sample was kept in the chamber overnight. Considerable differences can be observed between these two spectra. The

Table 2
Assignment of Ce 3d peaks in XPS

		v_0	v	v′	v″	v‴
Ce $3d_{5/2}$	Origin	Ce^{3+}	Ce^{4+}	Ce^{3+}	Ce^{4+}	Ce^{4+}
	Shift (eV)	−36.1	−34.1	−30	−27.85	−18.3
	FWHM	4.11	5.77	3.76	2.69	3.96
		u_0	u	u′	u″	u‴
Ce $3d_{3/2}$	Origin	Ce^{3+}	Ce^{4+}	Ce^{3+}	Ce^{4+}	Ce^{4+}
	Shift (eV)	−17.8	−15.65	−13.65	−9.25	0
	FWHM	3.91	5.86	4.00	4.64	1.39

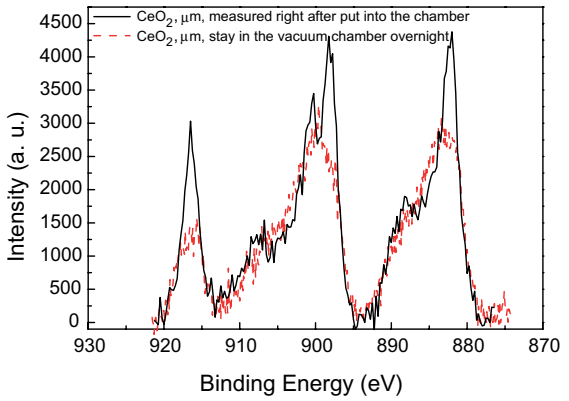

Fig. 2. Two XPS spectra of micron-sized cerium oxide. The dotted line was measured right after the sample was loaded into the UHV chamber (a); the solid line was measured after the sample remained overnight in UHV chamber. The solid spectrum is close to the spectrum in Fig. 1(b), while the dotted line spectrum is similar to the one in Fig. 1(a).

spectrum taken immediately after loading the sample into the chamber is nearly identical to the spectrum of CeO_2, while the spectrum taken after being held in UHV overnight is similar to the spectrum for Ce_2O_3 in Fig. 1. The results from simulating both spectra give Ce^{3+} concentrations of 11.6% for the sample measured immediately after sample-loading and 29.3% for the sample measured after overnight storage in the chamber. Henceforth we use sample "one" and sample "two" to denote these two samples.

The Ce^{3+} concentrations measured for nanoparticles are listed in Table 3 in the column denoted XPS surface Ce^{3+} concentration. For the nanoparticle results, XPS spectra were measured immediately after the samples were loaded into the UHV chamber with an acquisition time of 60 min.

3.2. X-ray absorption near edge spectroscopy

As shown in Fig. 3, there are four peaks in a typical ceria XANES spectrum obtained at the Ce L_{III} edge. The four observed peaks in the Ce L_{III} edge XANES have been reported and assigned previously [20–22]. Peak A is a Ce^{4+} peak with the final state of $2\underline{p}4f^0 5d^1$, which denotes that an electron is excited from the Ce 2p shell to its 5d shell, and there is no electron in the 4f shell. Peak B is also a Ce^{4+} peak, with the final state of $2\underline{p}4f^1 5d^1 v$, which denotes that in addition to an electron excited from Ce 2p shell to 5d shell, another electron is also excited from the valence band (O 2p shell) to Ce 4f shell, leaving a hole

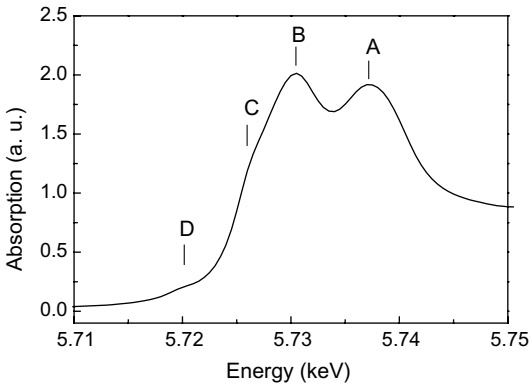

Fig. 3. A typical Ce L_{III} edge XANES spectrum of CeO_2 showing features of A, B, C and D.

Table 3
Ce^{3+} concentrations in ceria nanoparticles and micron-size particles from XPS and XANES

Particle size (nm)	XPS			XANES	
	Surface [Ce^{3+}] (%)	Shell layer thickness Δd (Å)	Bulk [Ce^{3+}] (%)	[Ce^{3+}] (%) estimated with subtraction method	[Ce^{3+}] (%) estimated with LC method
6	25.2	2.2	10.6	6	7
10	22.3	1.9	5.6	1	1
5000	11.6	0.9	0.0054	0[a]	0[a]
5000 (Overnight)	29.3	2.6	0.016	N/A	N/A

XPS surface results are used to estimate the corresponding bulk concentrations and the shell thickness using a core–shell model.
[a] Note: Micron-sized CeO_2 was used as a standard for 100% Ce^{4+} and 0% Ce^{3+}.

(represented with v above) in the valence band. Peak C is a Ce^{3+} peak, and peak D is a pre-edge peak, for which the electron excitation mechanism remains unclear.

Most XANES studies on cerium oxide are qualitative, and are usually applied to monitor the growth or sintering effects of the nanomaterials [23–25]. Peak fitting methods have been applied to estimate Ce^{3+} concentrations [25]. The observed peaks in Ce L_{III} XANES spectra were fitted with Gaussian functions. An arctan function was applied to simulate the continuum edge jump in the spectra. The Ce^{3+} concentration was then determined from the spectral weight of peak C. However, it is difficult to determine the position of the edge jump. The accuracy of such estimation was low until Overbury et al. [26] provided a quantitative method to study the Ce^{3+} concentration in ZrO_2-doped ceria. Overbury found that in a reducing environment, while increasing the temperature from room temperature to 680 °C, the heights of peaks A, B, and C changed in the Ce L_{III} edge spectra of $Ce_{0.7}Zr_{0.3}O_2$. Higher reduction temperature resulted higher peak C, and lower peaks A and B. The Ce^{3+} concentration was estimated by subtracting a standard Ce^{3+} spectrum from the measured Ce L_{III} edge XANES spectra of the ZrO_2-doped CeO_2 samples and comparing the corresponding height differences of peak C and peak A in the difference spectra.

Fig. 4(a) shows the XANES spectra of cerium oxide for different particle sizes measured at the Ce L_{III} edge. In Fig. 4(b), a corresponding region of Ce_2S_3 spectrum is subtracted from each spectrum. Compared to the spectra with micron-sized particles, the 6 nm ceria spectrum has a higher C peak and a lower A peak. By using this spectrum-subtracting method (described in [25], henceforth called subtraction method), the Ce^{3+} concentrations are calculated and listed in Table 3. More significant change can be found in peak B in Fig. 4(b). Peak B has a final state of $2\underline{p}4f^1 5d^1 v$, which reflects the interaction of Ce–O bonding. Cerium oxide is an ionic material. Stronger ionic Ce–O bonds yield a more intense B peak. The Ce^{4+} ion has a higher ionicity than that of Ce^{3+} ion. If Ce^{3+} replaces Ce^{4+}, the ionic bonding between cerium and oxygen becomes smaller, decreasing the intensity of peak B. Based on band theory, the 4f shell of cerium in CeO_2 can be treated as an impurity band between the valence band and the conduction band, while the 4f shell of cerium in Ce_2O_3 is a fully localized core state [27]. Therefore, $2\underline{p}4f^1 5d^1 v$ is a forbidden state in Ce_2O_3. The decrease of B peak also implies that there is a higher concentration of Ce^{3+} ions in the smaller nanoparticles. This observation is consistent with the observation that larger particles show a stronger intensity for peak B.

A linear component (LC) fitting method was used to estimate the concentration of Ce^{3+} in ceria nanoparticles as well. Under the assumption that an XANES spectrum of ceria nanoparticles at the Ce L_{III} edge is composed of a linear combination

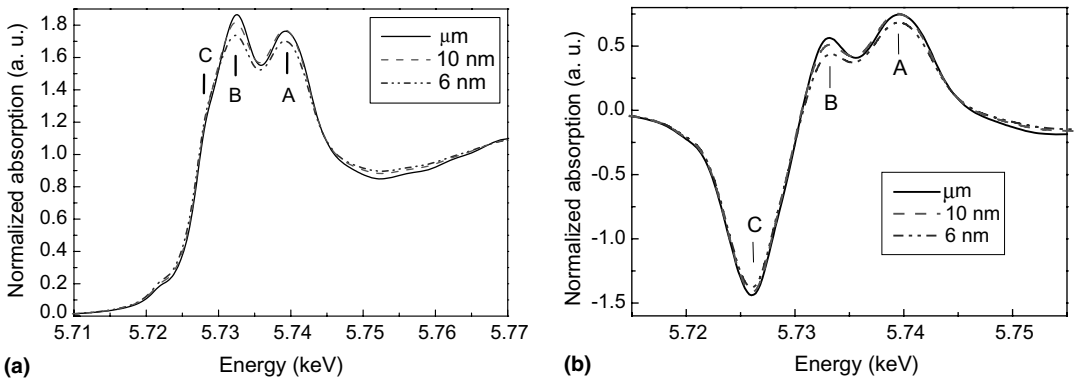

Fig. 4. (a) XANES spectra of cerium oxide with different particle size measured at Ce L_{III} edge. (b) Subtracting a standard Ce_2S_3 XANES spectrum from the spectra in (a).

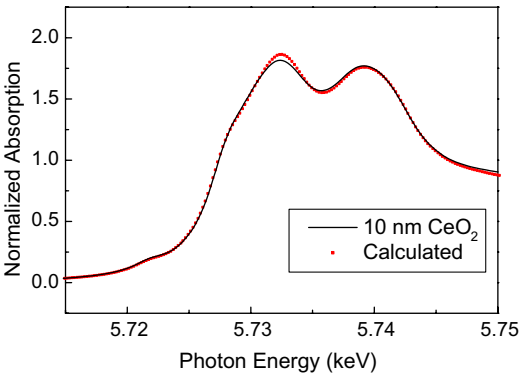

Fig. 5. Linear Component simulation of the XANES spectrum of 10 nm CeO_2 nanoparticle.

of a standard Ce^{4+} (micron-sized CeO_2) spectrum and a standard Ce^{3+} (micron-sized Ce_2S_3) spectrum, the percentage of Ce^{3+} can then be calculated from the weight factor of the Ce^{3+} spectrum,

$$I_{CeO_2\text{–nano}} = f_1 \times I_{CeO_2\text{–micron}} + f_2 I_{Ce_2S_3} \quad (4)$$

$$[Ce^{3+}] = \frac{f_2}{f_1 + f_2} \times 100\% \quad (5)$$

where $I_{CeO_2\text{–nano}}$, $I_{CeO_2\text{–micron}}$, and $I_{Ce_2S_3}$ are the intensity of Ce L_{III}-edge XANES of nanocrystalline CeO_2, micron-sized CeO_2, and Ce_2S_3 respectively. f_1 and f_2 are the weighting factor of micron-sized CeO_2 and Ce_2S_3 spectra respectively. An LC simulation is shown in Fig. 5 with the results listed in Table 3. From Fig. 5, the simulated spectrum agrees well with the measured spectrum except for peak B. This exception is acceptable because the micron-sized CeO_2 has a higher B peak than that of ceria nanoparticles, as shown in Fig. 4. The Ce^{3+} concentrations calculated from the LC method also agree with the results based on the spectrum-subtraction method, as shown in Table 3.

4. Discussion

Ceria-based materials are famous for their redox properties, because of the conversion between Ce^{3+} and Ce^{4+} valence states under oxidation and reduction conditions. Many researchers have demonstrated the reduction of ceria at high temperature [9,29–32]. With the help of in-situ high temperature time-resolved XRD studies, Rodriguez [29,30,33] showed the lattice parameter change of ceria-based materials under oxidation and reduction. In reducing conditions, the lattice expands, while in oxidizing conditions, the lattice shrinks. The lattice expansion of ceria nanoparticles has been demonstrated by several groups [12,34–36]. By decreasing the particle size, the lattice parameter of ceria increases. Zhou [35] and Kamruddin [36] compared their lattice expansion results with those of Tsunekawa [34] and Zhang's [12]. The results of Zhou, Kamruddin, and Zhang's agree well with each other and are smaller than that of Tsunekawa's. Most authors explained this unusual lattice expansion with the formation of Ce^{3+} ions in the nanoparticles.

We have calculated the Ce^{3+} concentration based on our lattice expansion study of ceria nanoparticles [12]. Assuming that the lattice expansion arises directly from the increased concentrations of oxygen vacancies and the larger Ce^{3+} ions with decreasing particle size, we use the earlier rare-earth doping results [28] where the increase of the CeO_2 lattice parameter per cation concentration was plotted with increasing trivalent rare-earth cation radius. Using the Ce^{3+} radius of 0.1143 nm, we calculate the corresponding concentrations of oxygen vacancies and Ce^{3+} ions from lattice parameters as shown in Table 4. The theoretical calculation reveals that part of the lattice expansion in nanocrystalline ceria comes from the nanosize effects, i.e. Madelung negative pressure [37]. The Madelung negative pressure explains 60% of the lattice expansion of nanocrystalline ceria. In the model, we assume that the bulk modulus remains unchanged with the particle size. However, high pressure XRD study showed that by decreasing the particle size, the bulk modulus increased [38]. Compared with the bulk modulus (K) of bulk ceria, 230 GPa, the bulk modulus of 9–15 nm ceria particles reported was about 328 GPa. If indeed K is larger in ceria nanoparticles, then the lattice expansion from the Madelung model is overestimated by about 1.4 times using "bulk" modulus. Therefore, the present average Ce^{3+} concentrations obtained from XANES, 1% and 6.5% for 10 and 6 nm particles are reasonable (see Table 4).

Table 4
Oxygen vacancy concentrations and Ce^{3+} concentrations with decreasing particle size calculated from the lattice expansion

Particle size d (nm)	Lattice parameter a (nm)	y in CeO_{2-y}	$[Ce^{3+}]$	$[Ce^{3+}]$ corrected with Madelung Model $w/K = 230$ GPa	Average XANES results
>5000	0.54087	0	0	0	N/A
15	0.54131	0.008	0.016	0.006	N/A
10	0.54152	0.013	0.026	0.011	0.01
7.4	0.54285	0.038	0.076	0.031	Not measured
6.1	0.54330	0.047	0.094	0.038	0.065

Ceria employed in the three way catalysts is well known for its ability to absorb and release oxygen according to the following reaction:

$$CeO_{2-y} + (y/2)O_2 \Longleftrightarrow CeO_2$$

As mentioned earlier, ceria loses surface oxygens when exposed to low oxygen partial pressure and when irradiated by Al Kα X-ray in the XPS UHV chamber. Since XPS is widely used for studying the surface properties of materials, many such surface studies of ceria may involve unrevealed surface reduction. Here, a core–shell model of a nanoparticle with a Ce_2O_3 outer shell and a CeO_2 inner core is adopted to interpret the recorded XPS spectra. The electron inelastic mean-free paths employed for Ce_{3d} photoelectrons are 12.3 Å (λ_1) for Ce_2O_3 and 10.9 Å (λ_2) for CeO_2 [25]. Based on the concentrations of Ce^{3+} obtained from XPS, the thickness of the Ce_2O_3 surface layer is estimated using the following equations:

$$\frac{Ce^{3+}}{Ce^{3+}+Ce^{4+}} = \frac{\int_0^{\Delta d} N e^{-\frac{x}{\lambda_1 \sin(\theta)}} dx}{\int_0^{\Delta d} N e^{-\frac{x}{\lambda_1 \sin(\theta)}} dx + \int_{\Delta d}^{\infty} N e^{-\frac{x}{\lambda_2 \sin(\theta)}} dx} = \frac{\lambda_1\left(1 - e^{-\frac{\Delta d}{\lambda_1 \sin(\theta)}}\right)}{\lambda_1\left(1 - e^{-\frac{\Delta d}{\lambda_1 \sin(\theta)}}\right) + \lambda_2 e^{-\frac{\Delta d}{\lambda_2 \sin(\theta)}}} \quad (6)$$

$$[Ce^{3+}]_{Bulk} = \frac{[Ce^{3+}]_{Surface} S \Delta d}{V} \quad (7)$$

Here, Δd is the thickness of the outer layer; λ_1 and λ_2 are the inelastic mean free paths for photoelectrons in Ce_2O_3 and CeO_2 respectively; θ is the take-off angle; N is the number density of Ce ions regardless of valence. The calculated thickness of the Ce_2O_3 layer ranges from 0.09 to 0.26 nm (see Table 3). If we assume that all the Ce^{3+} are in outer layer of the particle only, the total "bulk" (i.e. particle volume average) concentrations of Ce^{3+} are then calculated from the Ce^{3+} surface concentrations (Table 3) based on Eq. (5), where S is the surface area, Δd is the thickness of the outer layer, V is the volume of the particle, $[Ce^{3+}]_{Bulk}$ and $[Ce^{3+}]_{Surface}$ are the Ce^{3+} concentration for the bulk and surface respectively. The "bulk" Ce^{3+} concentrations obtained by XPS analysis with the core–shell modeling are much lower than the "surface" Ce^{3+} concentrations directly from XPS measurements. These "bulk" Ce^{3+} concentrations agree more favorably with those of XANES, which are volume average results. The results indicate that one must be cautious if using XPS for quantitative analysis. Particularly, understanding the concentration depth profile of the elements is difficult in many cases. However, the "bulk" Ce^{3+} concentrations obtained using the core–shell model analysis from XPS measurements are still significantly larger than those obtained from XANES, especially for nanoparticles. For example, in the 10 nm sample, the "bulk" Ce^{3+} concentration from XPS is still 5 times higher than that obtained from XANES. The elevated surface concentrations obtained are most likely the result of surface reduction of Ce^{4+} in high vacuum chamber, a process that is enhanced by faster reaction kinetics at nanoparticle surfaces. This XPS phenomenon, however, can be exploited in dynamic reduction and oxygen diffusion studies once proper calibration is performed.

5. Conclusions

XPS is a powerful surface characterization tool that is used herein to determine the percentage of

Ce^{3+} in CeO_{2-x} nanoparticles. The data obtained from XPS, however, must be treated carefully. Three factors need to be taken into consideration when XPS is applied to determine the percentage of the Ce^{3+} in cerium oxide. First, XPS is an integral technique; the signals measured are related to the Laplace transform of the actual concentration depth profile. As a result, measured concentrations represent a weighted average of the concentration depth profile and must be interpreted with an appropriate model in order to determine true concentration depth profiles. In the present study, we employ a core–shell model to interpret the concentration depth profile of Ce^{3+} at the nanoparticle surface. The Ce^{3+} concentrations obtained from the XPS core–shell model analysis are significantly larger than those obtained from XANES experiments. This result points to the second important consideration: the placement of ceria particles within the XPS UHV chamber and the X-ray radiation may cause gradual reduction of Ce^{4+}. Herein, the concentration of Ce^{4+} decreased significantly after overnight storage inside the XPS chamber. Even for XPS samples measured immediately after loading, the concentration of Ce^{4+} obtained is significantly smaller than that obtained from XANES, particularly for nanoparticles. Finally, XPS can only yield information pertaining to the top several nanometers of the sample due to the small inelastic mean free paths of photoelectrons. Even for nanoparticles, the sampling depth can be considerably smaller than the particle diameter. Caution must therefore be exercised when estimating bulk compositions from XPS data. Higher concentrations of Ce^{3+} may have been reported in previous XPS studies due to the unintended and undetected surface reduction of ceria. A model for the composition depth profile is again required for this purpose.

We have also successfully shown that XANES, which does not need a vacuum, can be reliably used to measure the concentrations of Ce^{3+} in ceria nanoparticles, providing quantitative analysis using either the linear-component (LC) method and/or the spectrum-subtraction method. The combination of XPS and XANES can be employed to study reduction dynamic and oxygen diffusion of oxide nanoparticles.

Acknowledgements

We thank Dr. Simon Bare from UOP LLC for his kind assistance with XANES measurements and suggestion of applying LC analysis. This work is supported primarily by the MRSEC Program of the NSF under Award Number DMR-0213574. Research carried out in part at the National Synchrotron Light Source, Brookhaven National Laboratory, which is supported by the US Department of Energy, Division of Materials Sciences, and Division of Chemical Sciences, under Contract No. DE-AC02-98CH10886.

References

[1] A. Trovarelli, Catalysis by Ceria and Related Materials, Imperial College Press, London, 2002.
[2] J.C. Summers, S. Van Houtte, D. Psaras, Appl. Catal. B 10 (1996) 139.
[3] S. Tsunekawa, T. Fukuda, A. Kasuya, Surf. Sci. 457 (3) (2000) L437.
[4] S. Tsunekawa, K. Ishikawa, Z.Q. Li, Y. Kawazoe, A. Kasuya, Phys. Rev. Lett. 85 (16) (2000) 3440.
[5] E. Paparazzo, G.M. Ingo, N. Zacchetti, J. Vac. Sci. Technol. A 9 (3) (1991) 1416.
[6] M.V. Rama Rao, T. Shripathi, J. Electron Spectrosc. Relat. Phenom. 87 (1997) 121.
[7] G. Liu, J.A. Rodriguez, J. Hrbek, J. Dvorak, J. Phys. Chem. B 105 (2001) 7726.
[8] H. Cui, G. Hong, X. Wu, Y. Hong, Mater. Res. Bull. 37 (2002) 2155.
[9] J.P. Holgado, G. Munuera, J.P. Espinós, A.R. González-Elipe, Appl. Surf. Sci. 158 (2000) 164.
[10] E. Paparazzo, Surf. Sci. 234 (1990) 1253.
[11] D.E. Ramaker, C.T. White, J.S. Murday, J. Vac. Sci. Tech. 18 (1981) 748.
[12] F. Zhang, S.-W. Chan, J.E. Spanier, E. Apak, Q. Jin, R.D. Robinson, I.P. Herman, Appl. Phys. Lett. 80 (1) (2002) 127.
[13] J.E. Spanier, R.D. Robinson, F. Zhang, S.-W. Chan, I.P. Herman, Phys. Rev. B 64 (2001) 245407.
[14] F. Zhang, Q. Jin, S.-W. Chan, J. Appl. Phys. 95 (8) (2004) 4319.
[15] R.D. Robinson, J.E. Spanier, F. Zhang, S.-W. Chan, I.P. Herman, J Appl. Phys. 92 (4) (2002) 1936.
[16] T. Ressler, WinXAS software, www.winxas.de (Version Nov. 2002).
[17] P. Burroughs, A. Hammett, A.F. Orchard, G. Thornton, J. Chem. Soc. Dalton Trans. 1976 (1976) 686.
[18] E.J. Preisler, O.J. Marsh, R.A. Beach, T.C. McGill, J. Vac. Sci. Tech. B 19 (4) (2001) 1611.
[19] J. Zhang, X. Ju, Z.Y. Wu, T. Liu, T.D. Hu, Y.N. Xie, Z.L. Zhang, Chem. Mater. 13 (2001) 4192.

[20] D.D. Beck, T.W. Capehart, R.W. Hoffman, Phys. Lett. 159 (1989) 207.
[21] A.V. Soldatov, T.S. Ivanchenko, S. Della Longa, A. Kotani, Y. Iwamoto, A. Bianconi, Phys. Rev. B 50 (8) (1994) 5074.
[22] J. el Fallah, S. Boujana, H. Dexpert, A. Kiennemann, J. Majerus, O. Touret, F. Villain, F. Le Normand, J. Phys. Chem. 98 (1994) 5522.
[23] Z. Wu, R.E. Benfield, L. Guo, H. Li, Q. Yang, D. Grandjean, Q. Li, H. Zhu, J. Phys.: Condens. Matter 13 (2001) 5269.
[24] S. Yamazaki, T. Matsui, T. Ohashi, Y. Arita, Solid State Ionics 136–137 (2000) 913.
[25] P. Nachimuthu, W.-C. Shih, R.-S. Liu, L.-Y. Jang, J.-M. Chen, J. Solid State Chem. 149 (2000) 408.
[26] S.H. Overbury, D.R. Huntley, D.R. Mullins, G.N. Glavee, Catal. Lett. 51 (3–4) (1998) 133.
[27] N.V. Skorodumova, R. Ahuja, S.I. Simak, I.A. Abrikosov, B. Johnasson, B.I. Lumdqvist, Phys. Rev. B 64 (2001) 115108.
[28] J.R. McBride, K.C. Hass, B.D. Poindexter, W.H. Weber, J. Appl. Phys. 76 (1994) 2435.
[29] J.A. Rodriguez, X.Q. Wang, J.C. Hanson, G. Liu, A. Iglesia-Juez, M. Fermandez-Garcia, J. Chem. Phys. 119 (11) (2003) 5659.
[30] J.A. Rodriguez, T. Jirsak, A. Freitag, J.C. Hanson, J.Z. Larese, S. Chaturvedi, Catal. Lett. 62 (2–4) (1999) 113.
[31] A. Tschope, R. Birringer, NanoStruc. Mater. 9 (1997) 591.
[32] K. Sohlberg, S.T. Pantelides, S.J. Pennycook, J. Am. Chem. Soc. 123 (2001) 6609.
[33] J.A. Rodriguez, J.C. Hanson, J.Y. Kin, G. Lui, A. Iglesias-Juez, M. Fermandez-Garcia, J. Phys. Chem. B 107 (15) (2003) 3535.
[34] S. Tsunekawa, R. Sivamohan, S. Ito, A. Kasuya, T. Fukuda, NanoStruc. Mater. 11 (1) (1999) 141.
[35] X.-D. Zhou, W. Huebner, Appl. Phys. Lett. 79 (2001) 3512.
[36] M. Kamruddin, P.K. Ajikumar, R. Nithya, A.K. Tyagi, B. Raj, Scripta Mater. 50 (2004) 417.
[37] V. Perebeinos, S.-W. Chan, F. Zhang, Solid State Commun. 123 (2002) 295.
[38] Z. Wang, S.K. Saxena, V. Pischedda, H.P. Kiermann, C.S. Zha, Phys. Rev. B 64 (2001) 012102.